

The Lyman Break Galaxies: their progenitors and descendants

Kentaro Nagamine

*Joseph Henry Laboratories, Physics Department, Princeton University,
Princeton, NJ 08544, USA*

nagamine@astro.princeton.edu

ABSTRACT

We study the evolution of Lyman Break Galaxies (LBGs) from $z = 5$ to $z = 0$ by tracing the merger trees of galaxies in a large-scale hydrodynamic simulation based on a Λ cold dark matter model. In particular, we emphasize on the range of properties of the sample selected by the rest-frame V band luminosity, in accordance with recent near-IR observations. The predicted rest-frame V band luminosity function agrees well with the observed one when dust extinction is taken into account. The stellar content and the star formation histories of LBGs are also studied. We find that the LBGs intrinsically brighter than $M_V = -21.0$ at $z = 3$ have stellar masses of at least $10^9 M_\odot$, with a median of $10^{10} h^{-1} M_\odot$. The brightest LBGs ($M_V \lesssim -23$) at $z = 3$ merge into clusters/groups of galaxies at $z = 0$, as suggested from clustering studies of LBGs. Roughly one half of the galaxies with $-23 \lesssim M_V \lesssim -22$ at $z = 3$ fall into groups/clusters, and the other half become typical L^* galaxies at $z = 0$ with stellar mass of $\approx 10^{11} M_\odot$. Descendants of LBGs at the present epoch have formed roughly 30% of their stellar mass by $z = 3$, and the half of their current stellar population is 10 Gyr old, favoring the scenario that LBGs are the precursors of the present day spheroids. We find that the most luminous LBGs have experienced a starburst within 500 Myr prior to $z = 3$, but also have formed stars continuously over a period of 1 Gyr prior to $z = 3$ when all the star formation in progenitors is coadded. We also study the evolution of the mean stellar metallicity distribution of galaxies, and find that the entire distribution shifts to lower metallicity at higher redshift. The observed sub-solar metallicity of LBGs at $z = 3$ is naturally predicted in our simulation.

Subject headings: stars: formation — galaxies: formation — galaxies: evolution — galaxies: high-redshift — cosmology: theory — methods: numerical

1. Introduction

A large sample of galaxies at $z = 3 - 4$ has become available owing to the observational technique of selecting high-redshift galaxies by broad-band color signatures when the Lyman limit spectral discontinuity at 912 \AA passes through different filters; the so-called Lyman Break Galaxies (LBGs; Steidel & Hamilton 1992; Steidel, Pettini, & Hamilton 1995). So far, most surveys have been carried out at optical wavelengths, which corresponds to LBGs in the rest-frame far ultra-violet (UV). Such observations have detected strong clustering of LBGs (Adelberger et al. 1998; Giavalisco et al. 1998; Steidel et al. 1998), which has generally been interpreted as indirect evidence that LBGs reside in massive dark matter halos.

However, the true character of LBGs and their evolutionary history remain uncertain. In one scenario, LBGs are low-mass, merger-induced starbursting systems, and are the precursors of present day low-mass spheroids (Lowenthal et al. 1997; Sawicki & Yee 1998; Somerville, Primack, & Faber 2001). In another scenario, they have stellar mass of $\approx 10^{10} M_{\odot}$, sitting in massive dark matter halos and continuously forming stars over a period of 1 Gyr. They evolve into bright elliptical and spiral galaxies at $z = 0$, and later merge into clusters or groups of galaxies (Mo & Fukugita 1996; Steidel et al. 1996; Baugh et al. 1998). Another possibility is that they are massive galaxies experiencing merger-induced starbursts (Somerville et al. 2001).

In order to clarify the stellar content and the star formation histories of LBGs, near infra-red (IR) studies of LBGs have recently been carried out (Sawicki & Yee 1998; Papovich, Dickinson, & Ferguson 2001; Pettini et al. 2001; Shapley et al. 2001; Rudnick et al. 2001). These observations directly probe the rest-frame optical properties of LBGs at $z = 3$; wavelengths less affected by dust obscuration. However, the number of galaxies used in these studies is still small, and the inferred star formation time-scale and the values of extinction differ somewhat among authors due to different sample selection and different modeling of SEDs used in their analyses. Nevertheless, the median value of extinction seems to lie in the range $E(B - V) \approx 0.1 - 0.3$, and the recent studies seem to indicate the existence of a significant old stellar population in LBGs at $z = 3$ with the stellar mass of $\approx 10^{10} M_{\odot}$ (Papovich et al. 2001; Shapley et al. 2001). In addition, Pettini et al. (2001) used the observed oxygen lines in the rest-frame optical to estimate the metallicity of LBGs to be $0.1 - 1.0 Z_{\odot}$.

In this article, we focus on the merger history and the star formation history of LBGs from $z = 5$ to 0, as well as their stellar content. We follow the merger trees of galaxies both backward and forward in time, and examine the stellar mass of progenitors and descendants of LBGs as well as their star formation histories. We hope to provide some insights on how LBGs fit into the overall galaxy formation picture in a cold dark matter (CDM) model; in particular, we address what kind of objects LBGs form from, and what type of objects LBGs

evolve into.

In our earlier papers (Nagamine, Fukugita, Cen, & Ostriker 2001a,b, hereafter Paper I and II), we discussed the star formation history, stellar metallicity distribution, luminosity function, and color distribution of galaxies in a Λ CDM universe using the same simulation. There we showed that the agreement between local observations and the simulation was relatively good, considering the uncertainties involved on both sides, and argued that we are beginning to obtain meaningful results for the global properties of galaxies in large-scale hydrodynamic simulations, with the hydrodynamic mesh approaching $\sim (1000)^3$. The simulation used in this paper has a box size of $L_{\text{box}} = 25h^{-1}$ Mpc with Eulerian hydrodynamic mesh of 768^3 and cosmological parameters of $(\Omega_m, \Omega_\Lambda, \Omega_b, h, \sigma_8) = (0.3, 0.7, 0.035, 0.67, 0.9)$ (See Paper I for the details of the simulation).

Other numerical studies of LBGs using hydrodynamic simulations exist. Davé et al. (1999) and Weinberg, Hernquist, & Katz (2000) used a Smoothed Particle Hydrodynamic (SPH) simulation with a box size of $11.1h^{-1}$ Mpc, which was stopped at $z = 2$, due to a lack of long wavelength perturbations. Therefore, they cannot check whether the properties of the simulated galaxies are consistent with local galaxy observations, in particular, the luminosity function, the color distribution of galaxies, and the stellar matter density at $z = 0$. On the other hand, the simulation used in this paper is continued up to $z = 0$. The advantage of SPH simulations is much higher spatial resolution than that of Eulerian simulations, but the SPH mass resolution is usually about an order of magnitude worse than that of the Eulerian method which is adopted in this paper. With these differences in the simulations, it is interesting to compare the results from the two types of simulations. Comparisons with the work of Davé et al. (1999) and Weinberg et al. (2000) will be discussed in the following sections. The present work extends and complements earlier works.

As in Paper II, we identify galaxies using the grouping algorithm HOP (Eisenstein & Hut 1998), and use the isochrone synthesis model GISSEL99 (Bruzual & Charlot 1993, Charlot 1999, private communication) to obtain the stellar luminosity output in the simulation. We assume an initial mass function of Salpeter (1955) with a turnover at the low-mass end as reported by Gould, Bahcall, & Flynn (1996).

In § 2, we describe how we select LBGs in our simulation. The rest-frame V band luminosity function of galaxies at $z = 3$ in the simulation is presented in § 3, which is compared with the observed one. We discuss the stellar mass of LBGs in § 4. The merger trees and the star formation histories of LBGs are presented in § 5 ($z \geq 3$) and § 6 ($z \leq 3$), and the progenitor masses and the fate of LBGs are discussed. The star formation rate of LBGs is studied in § 7, with emphasis on instantaneous vs. continuous star formation. In § 8, we discuss the metallicity of LBGs and the evolution of the entire luminosity-metallicity

relation. We conclude in § 9.

2. Selection of LBGs

Observers select galaxies efficiently at $z \sim 3$ by using a color selection criteria in color-color space (e.g. with U_n, G, \mathcal{R} filters; Steidel et al. 1999). By doing so, they select out star forming galaxies that are bright in far-UV at $z \sim 3$. Therefore, it is often assumed that LBGs have similar properties to the local starburst galaxies. Based on this expectation, many authors use an empirical extinction law of local starburst galaxies (e.g. Calzetti 1997) to model the internal dust extinction in these galaxies.

If we were to mimic the observational color-selection criteria, we would need to obtain the extinction $E(B - V)$ for each galaxy with some assumptions; for example, its proportionality to the metallicity and the star formation rate of each galaxy. An empirical extinction law for the wavelength dependence (e.g. Galactic, Small Magellanic Cloud, or starburst) also has to be assumed. The position of galaxies in a color-color space depends significantly on the effect of dust extinction, which is highly uncertain, and therefore the selection of galaxies will depend on the assumptions made for the calculation of $E(B - V)$ and the assumed extinction law. In particular, galaxies which have very high star formation rate may be strongly obscured and do not satisfy the color-selection criteria in the model. However, in reality, it is not clear how strongly these star-forming galaxies are obscured (e.g. there may be less obscuration due to the sweeping of dust clouds by galactic winds (Pettini et al. 2001; Aguirre et al. 2001)). Therefore, those galaxies which do not pass the color-selection criteria after dust extinction in the simulation may well be detected in reality within the current magnitude limit in the rest-frame V band given that they are also intrinsically bright in the optical wavelengths as we show in Figure 1.

In the left panel of Figure 1, we plot the computed rest-frame V band luminosity and the rest-frame far-UV luminosity (summing all flux below 1700\AA) of galaxies at $z = 3$ in our simulation before taking dust extinction into account (i.e. the intrinsic luminosity). The magnitude limit of $M_V < -21.0$ (which roughly corresponds to $K_s = 22.5$ of the near-IR observations by Shapley et al. (2001) with $h = 0.67$) is indicated by the vertical short-dashed line and the arrow to the right. The horizontal long-dashed line and the upward arrow roughly indicate the far-UV selection criteria of $\mathcal{R} < 25.5$ (Shapley et al. 2001). Note that the rest-frame V band selected sample includes a broad range of values of far-UV luminosity. Most current near-IR samples are first selected in the rest-frame far-UV, and then in the near-IR, therefore they are drawn from the upper right corner of this diagram (Sawicki & Yee 1998; Papovich et al. 2001; Shapley et al. 2001). However, near-IR selected

samples are becoming available (Rudnick et al. 2001), and there will be more in the future.

Therefore, rather than introducing further uncertainties in our analysis by invoking a certain color-selection criteria, here we consider all galaxies that are brighter than $M_V = -21.0$, and investigate the range of properties of the luminous galaxies at $z = 3$. But we do estimate the effect of dust extinction by making a few assumptions. In the right panel of Figure 1, we show the same luminosity distribution after applying a dust extinction model as follows: (i) The value of $E(B - V)$ is proportional to the star formation rate and the metallicity of each galaxy: $E(B - V) = \beta_{dust}(SFR/\langle SFR \rangle)(Z/Z_{max})^p$. The values of β_{dust} , $\langle SFR \rangle$, and p are adjusted so that the median $E(B - V)$ is 0.15, as suggested by Shapley et al. (2001)¹ (ii) The Calzetti et al. (2000) extinction law $k(\lambda)$ is assumed, where $F_{\lambda,observed} = F_{\lambda,intrinsic}10^{-0.4k(\lambda)E(B-V)}$. The function $k(\lambda)$ is obtained empirically from local starburst galaxies, and the function F_{λ} is the spectral energy distribution of galaxies.

The decrease in the V band luminosity is smaller than that in the far-UV luminosity, as the extinction law $k(\lambda)$ is a decreasing function of wavelength. Galaxies that are brighter than $M_V = -21.0$ after dust extinction are indicated by the empty squares in the right panel of Figure 1. The same galaxies are indicated by the same symbol in the left panel. The scatter of the points is somewhat larger in the right panel, and the most far-UV luminous galaxies in the left panel have moved to lower far-UV luminosity in the right panel because of the assumed proportionality between $E(B - V)$ and the star formation rate.

3. Rest-frame V Band Luminosity Function of LBGs at $z = 3$

In Figure 2, we show the computed rest-frame V band luminosity function of galaxies at $z = 3$ in the solid histogram (before dust extinction). The Schechter function fits at $z = 0, 3$, and 5 are shown as the short-dashed, solid, and long-dashed curves, respectively. The method for the Schechter fit is as follows: first we fix the faint-end slope to $\alpha = -1.15$ (This value is consistent with the empirical one in B band at $z = 0$. See Paper II.), then adjust the normalization Φ^* to fit the plateau at the faint end of the luminosity function, and then choose the characteristic magnitude M_V^* so that the integral of the Schechter function is equal to the total V band luminosity density in the simulation box. This fitting method is adopted to take into account of the luminosity of a few overmerged objects in the simulation

¹To avoid over-extincting high SFR galaxies, we adopt following sets of values after fixing $p = 0.2$ and $Z_{max} = 0.75$: $\beta_{dust} = (1.5, 1.5, 0.2, 0.2)$ and $\langle SFR \rangle = (790, 200, 50, SFR)$ for galaxies with $SFR[M_{\odot}/yr] = (> 200, 200 - 50, 50 - 10, 10 - 0)$. The SFRs used here were calculated with the time interval of 200 Myr. The median extinction value resulting from this prescription is $E(B - V) = 0.15$.

(see Paper II). At $z = 3$, we obtain $\Phi^* = 2.70 \times 10^{-2} h^3 \text{Mpc}^{-3}$ and $M_V^* = -22.05$ ($h = 0.67$). The Schechter parameters at other redshifts are summarized in Table 1. Similar table in the rest-frame B band was reported in Paper II. The dotted histogram is the luminosity function after applying the dust extinction model described in § 2. When the same fitting procedure is applied to the dotted histogram, it gives $\Phi^* = 2.70 \times 10^{-2} h^3 \text{Mpc}^{-3}$ and $M_V^* = -21.28$ ($h = 0.67$). Shapley et al. (2001) report the Schechter parameters of the rest-frame V band luminosity function of LBGs to be: $\alpha = -1.85 \pm 0.15$, $M_V^* = -22.21 \pm 0.25 + 5 \log h$, and $\Phi^* = (0.18 \pm 0.08) \times 10^{-2} h^3 \text{Mpc}^{-3}$, which is shown as the thick solid line in Figure 2.

At the bright end of the luminosity function, the agreement between the dust extinguished computed luminosity function (dotted) and the observed one (thick solid) is very good. This suggests that the intrinsic value of Φ^* could be much larger than that given by Shapley et al. (2001). The observational estimate of the faint end slope $\alpha = -1.85$ is significantly steeper than the simulated result, but this is perhaps due to the fact that they have only observed the bright end of the luminosity function. Our result suggests that, with the magnitude limit of $M_V \sim -21$, one is not seeing the faint-end of the luminosity function sufficiently at $z = 3$, and dust extinction exacerbates the situation. Therefore it is observationally difficult to derive the Schechter parameters correctly with the current detection limit.

A further detailed comparison of the parameters M_V^* and Φ^* is meaningless because of the huge covariance between α , M^* , and Φ^* . What counts here is the luminosity function itself, rather than the exact value of Schechter parameters. We consider that the agreement between the simulated and the observed luminosity function is fair given the uncertainties involved in the theoretical modeling of the simulation and observations. We remark that, in Paper II, we found a similar level of agreement in the rest-frame B band at $z = 0$ between the simulated luminosity function and the empirical estimates by the Sloan Digital Sky Survey (Blanton et al. 2000) and the 2dF survey (Cross et al. 2001). It is encouraging that we get this level of agreement between the simulation and the observations without any fine-tuning of the parameters of the simulation.

Our simulation predicts a rest-frame V band comoving luminosity density of $\mathcal{L}_V = 7.6 \times 10^8 h L_{\odot,V} \text{Mpc}^{-3}$ (before extinction) and $3.8 \times 10^8 h L_{\odot,V} \text{Mpc}^{-3}$ (after extinction), when the luminosity of all the galaxies in the simulation is summed up. If the sum is taken only for the galaxies above the detection limit of $M_V = -21.0$, we get $4.7 \times 10^8 h L_{\odot,V} \text{Mpc}^{-3}$ (before extinction) and $1.7 \times 10^8 h L_{\odot,V} \text{Mpc}^{-3}$ (after extinction). Shapley et al. (2001) give $\mathcal{L}_V = 1.35 \times 10^8 h L_{\odot,V} \text{Mpc}^{-3}$ by integrating the observationally inferred luminosity function to the same detection limit. The last two values above are consistent with each other when uncertainties in both sides are considered. Further detailed comparison of total luminosity density is hindered by the current detection limit. We remark that the predicted B band

luminosity density and the stellar mass density at $z = 0$ in our simulation are consistent with the empirical estimates within the uncertainties (see Paper II).

Davé et al. (1999) calculated the R band luminosity function by assuming a galactic extinction law with fixed $A_V = 1.0$ for all galaxies in a SPH simulation, and argued that the result is in rough agreement with the observed luminosity function when dust extinction is taken into account, although the simulated luminosity function was somewhat steeper. A detailed comparison of Schechter parameters was not presented in their paper.

4. Stellar Mass of LBGs

In our simulation, the luminosity and stellar mass of galaxies correlate well, as shown explicitly in Figure 3. In each panel, the dashed lines are drawn by hand to roughly indicate the locus of the distribution, together with the value of the constant C , where $\log M_{\text{stellar}} = -0.4M_V + C$ and M_{stellar} is in units of $[h^{-1}M_{\odot}]$. The entire distribution shifts to the upper left from high to low redshift, as galaxies become more massive and less luminous with time on average. The scatter in the distribution is larger at higher redshift, reflecting the younger age of stars and the variety in the star formation histories of high-redshift galaxies relative to low-redshift ones.

In the $z = 3$ panel, the detection limit of $M_V = -21.0$ (Shapley et al. 2001) is indicated by the vertical solid line and the arrow. The intersection of the solid and the dashed lines indicates that the currently observed LBGs have stellar masses of at least $10^9 h^{-1} M_{\odot}$, and those at the detection limit are in the range $10^9 - 10^{10} h^{-1} M_{\odot}$. The median stellar mass of all galaxies that are brighter than $M_V = -21.0$ is $10^{10} h^{-1} M_{\odot}$. When dust extinction is taken into account, the distribution becomes dimmer by about a magnitude, and the mass range at the magnitude limit shifts upward slightly: $10^{9.5} - 10^{10.5} h^{-1} M_{\odot}$. Our result is consistent with the derived stellar mass by Shapley et al. (2001).

5. Merger Trees and Star Formation Histories of LBGs at $z \geq 3$

In Figure 4, we show the merger trees of some of the brightest LBGs at $z = 3$ in the simulation in the order of their rest-frame V band luminosity at $z = 3$ (galaxy ID [gid]= 0, 30, 3, 96, 33, 2). All of these galaxies are also bright in the rest-frame far-UV, and should be visible in the current far-UV selected galaxy observation as well. The figure shows the stellar mass of galaxies at $z = 3, 4$, and 5 in the ordinate. The merger events are shown by connecting the points at each epoch. Note that the actual merger events might have

taken place anytime between the two redshifts.

In Figure 5, we show the composite star formation histories of the progenitors which end up in these LBGs, in the decreasing order of the rest-frame V band luminosity from top to bottom. In each panel, the values of stellar mass (in units of M_{\odot}) and rest-frame V band absolute magnitude of each object at $z = 3$ are indicated. The bin size of the histogram is 50 Myr.

Now let us describe several selected objects more closely.

The galaxy $\text{gid}=0$ is the most massive and the brightest object in the simulation at $z = 3$, and has $M_{\text{stellar}} = 3.78 \times 10^{11} h^{-1} M_{\odot}$. It might be suffering from the overmerging problem at $z = 3$ (i.e. could be a few separate objects in reality). It has experienced multiple merger events from $z = 5$ to $z = 3$. Its star formation history (top panel of Figure 5) tells us that the progenitors of this object have continuously formed stars from $z = 10$ to $z = 4$. It has experienced a significant starburst in between $z = 4$ and $z = 3$ which lasted over a period of 100 Myr. This galaxy grows into a group of galaxies with $M_{\text{stellar}} = 2.6 \times 10^{12} h^{-1} M_{\odot}$ at $z = 0$, as we will see in the next section.

The galaxies $\text{gid}=30$, 3, and 96 all merge into a same cluster at $z = 0$ with $M_{\text{stellar}} = 6.0 \times 10^{12} h^{-1} M_{\odot}$, as we will show in the next section. Interestingly, $\text{gid}=30$ has the smallest stellar mass among the three, but it is the brightest because it had a starburst closer to $z = 3$ than the other two.

The galaxy $\text{gid}=96$ offers an interesting example, where we see a major starburst at $z = 3 - 4$ but no corresponding major merger event during the same period. A significant gas infall without a galaxy merger event must have taken place in this case. This galaxy only experiences two merger events in the interval $z = 4 - 5$ and $z = 5 - 6$.

The galaxy $\text{gid}=33$ is interesting because it grows into a galaxy of $M_{\text{stellar}} = 1.9 \times 10^{11} h^{-1} M_{\odot}$ at $z = 0$, a Milky Way sized galaxy with the color of $B - V = 0.82$, typical of a S0a galaxy (Roberts & Haynes 1994). It experiences a moderate number of merger events at $z > 3$, and has continuously formed stars over a period of 1 Gyr.

The galaxy $\text{gid}=2$ is also interesting in that it has almost no star formation activity in the interval $z = 3 - 4$, but is still bright enough at $z = 3$ because of the significant star formation at $z > 4$ associated with multiple merger events. This object merges into the same group at $z = 0$ as $\text{gid}=0$ does.

To summarize, the majority of LBGs that are intrinsically brighter than $M_V = -23$ at $z = 3$ have experienced intensive star formation activities ($\geq 100 M_{\odot}/\text{yr}$) within 500 Myr prior to $z = 3$, often lasting for a period of ~ 100 Myr, resulting in a stellar mass of

$> 10^{10}M_{\odot}$. Besides the starbursts, the progenitors of these bright LBGs have continuously formed stars over a period of 1 Gyr since $z = 10$ when they are coadded. Qualitatively, these histories seem to be consistent with the star formation histories inferred from recent near-IR observations of LBGs (Papovich et al. 2001; Pettini et al. 2001; Shapley et al. 2001). Most of the starbursts in the simulation seem to be associated with merger events, but this is not necessarily so, as in the case of gid=96. Milder gas infall not associated with a merger event has taken place in such cases. At $z = 5$, the stellar mass of the progenitors of LBGs ($M_V < -21.0$ at $z = 3$) ranges from $10^{6.9}h^{-1}M_{\odot}$ to $10^{10.8}h^{-1}M_{\odot}$, with the median value of $10^{8.6}h^{-1}M_{\odot}$.

6. The Fate of LBGs at $z \leq 3$

6.1. Merger Tree and Star Formation History

In Figure 6, we show the merger histories of representative objects which end up as clusters (panels A & B), groups (panels C & D), and L^* galaxies (panels E & F) at $z = 0$. The LBGs that are brighter than $M_V = -21.0$ are indicated by the crosses at $z = 3$. Some of the brightest LBGs that were described in Figure 4 are indicated by the open squares at $z = 3$, with their galaxy IDs on the side. The open circles in panels (A)–(D) indicate that the objects are suffering from the overmerging problem in the simulation, and represent clusters/groups of galaxies as a whole.

The panels (A) and (B) show that a present day cluster of galaxies contains roughly $\gtrsim 10$ LBGs as their progenitors, as indicated by the crosses at $z = 3$ in the figure. They continue to collect numerous less massive objects with $M_{\text{stellar}} = 10^7 - 10^9 M_{\odot}$ at $z = 0 - 3$. We find that the majority of LBGs that are intrinsically brighter than $M_V = -23$ at $z = 3$ merge into clusters/groups of galaxies at $z = 0$ in our simulation.

The panels (C) and (D) show that a present day group of galaxies typically contains one to $\lesssim 10$ LBGs as their progenitors. We find that roughly one half of LBGs with $-23 \lesssim M_V \lesssim -22$ merge into groups/clusters of galaxies, while the other half evolve into typical L^* galaxies with $M_{\text{stellar}} \sim 10^{11}M_{\odot}$ as shown in the panels (E) and (F). Present day galaxies with $M_{\text{stellar}} \gtrsim 10^{11}M_{\odot}$ typically have one to a few LBGs as their precursors which are brighter than $M_V = -21.0$ and have $M_{\text{stellar}} \gtrsim 10^{10}M_{\odot}$ at $z = 3$.

The corresponding composite star formation histories for all cases are presented in Figure 7 as functions of the age of the universe and redshift. The exceptionally high star formation rates seen for (A), (B), and (C) are because these histograms are the composite of all progenitors which later fall into the same cluster/group. The stellar mass of the object

at $z = 0$ is indicated in each panel.

One sees that the star formation activity is more episodic at lower redshifts. In very massive systems (panels A–C), we see no quiescent star formation at low-redshift, which agrees with the observed absence of star formation in clusters of galaxies at late times. This is presumably due to the inefficient cooling of the gas in massive systems because of the high temperature of the shock-heated gas (Rees & Ostriker 1977; Silk 1977; Blanton et al. 1999).

Panel (D) has relatively frequent star formation activity up to $z \sim 0.2$. It only contains a single LBG which is brighter than $M_V = -21.0$ at $z = 3$. The total stellar mass of this system at $z = 0$ is $3.15 \times 10^{11} h^{-1} M_\odot$, with a color of $B - V = 0.86$, typical of a S0 galaxy (Roberts & Haynes 1994).

Panel (E) offers an interesting example of a system with stellar mass of $\sim 2 \times 10^{11} h^{-1} M_\odot$ at $z = 0$, with a color of $B - V = 0.82$, typical of a S0a galaxy (Roberts & Haynes 1994). Despite of the multiple accretion of small systems up to the present epoch, it hardly forms stars at $z < 1$. It contains a few LBGs ($M_V < -21.0$) as its precursor at $z = 3$.

A counter-example to (E) is shown in panel (F), where more star formation activity is seen with less merger events when compared with (E). This system has only one LBG as its precursor at $z = 3$, and this LBG remains untouched until $z = 1$. Major merger events take place at $z < 0.5$, inducing significant star formation, and the stellar mass of the system increases dramatically at $z < 0.5$.

6.2. Spheroids as the Descendants of LBGs

In Figure 8, we show the cumulative stellar mass fraction as a function of the age of the universe for the total box (short dashed), descendants of the LBGs which are brighter than $M_V = -21.0$ at $z = 3$ (solid), and the cluster shown in panel (A) of Figure 6. The long dashed lines indicate two epochs: $z = 3$ and $t = 4$ Gyr, where t is the age of the universe. The intersections with the solid curve show that the descendants of LBGs today have formed $\sim 30\%$ of their stellar mass by $z = 3$, and $\sim 50\%$ by $t = 4$ Gyr. In other words, 50% of the present day stellar population in LBG descendants is 10 Gyr old. Together with the merger trees presented in the previous subsection, this suggests that the stars we see as LBGs at $z = 3$ will evolve into massive old stellar component of the present day galaxies; i.e. the ‘spheroids’ (bulges of spirals and luminous ellipticals). The observed compactness of LBGs ($\lesssim 4$ kpc; Lowenthal et al. 1997; Giavalisco et al. 1996) is consistent with this idea. Many authors also prefer the spheroid scenario to the low-mass starburst scenario (Lowenthal et al. 1997) and the satellite starburst (Somerville et al. 2001) from other considerations, such

as a chemodynamical model which combines chemical evolution model with 1 dimensional hydrodynamics (Friaca & Terlevich 1999), or a semianalytic model which predicts sizes, kinematics, and star formation rates of LBGs (Mo, Mao, & White 1999).

Unfortunately, due to limited spatial resolution of our simulation, we cannot address the question of what happens to the LBGs that fall into clusters. Governato et al. (2001) have explored this issue by combining a semianalytic galaxy formation model with a high-resolution N-body simulation of a cluster. They find that the descendants of LBGs in clusters can be identified with a central cD galaxy and giant elliptical galaxies within the central 60% of the virial radius of a cluster.

7. Star Formation Rate of Galaxies: Instantaneous vs. Continuous

In Figure 9, we show the instantaneous star formation rate of galaxies at $z = 0, 1, 3,$ and 5, calculated by averaging over 20 Myr at each epoch, as a function of rest-frame V band absolute magnitude (before dust extinction). We have confirmed that the result is robust against the change in the time-scale of the averaging. Those which are assigned $\text{SFR} = 10^{-4}[h^{-1}M_{\odot}/\text{yr}]$ happen to have no star formation at that particular epoch, due to the intermittent nature of the star formation in the simulation. Note that ongoing star formation due to recycled matter within a galaxy might not be captured in this simulation due both to limited spatial resolution and the nature of the star formation recipe implemented in the simulation. The vertical dashed line at $z = 3$ indicates the detection limit of $M_V = -21.0$ (Shapley et al. 2001).

There is a relatively strong correlation between the instantaneous SFR and the luminosity of galaxies at $z \gtrsim 3$: more luminous galaxies are forming stars more actively. Because of the correlation between luminosity and stellar mass shown in Figure 3, this means that more massive galaxies are forming stars more actively on average in our simulation. Galaxies that are brighter than $M_V = -21.0$ take a wide range of instantaneous SFR; from $1M_{\odot}/\text{yr}$ to a few $100M_{\odot}/\text{yr}$. Galaxies at the detection limit have values ranging from $1M_{\odot}/\text{yr}$ to $\sim 30M_{\odot}/\text{yr}$. At lower redshifts ($z \leq 1$), star formation becomes inactive on average, as was shown in Paper I.

In Figure 10, we plot ‘Instantaneous SFR(20Myr)’ (averaged over 20 Myr) vs. ‘Continuous SFR(200Myr)’ (averaged over 200 Myr) of galaxies in the simulation. The diagonal solid line indicates where the two SFRs take the same value; i.e. the star formation is continuous over at least 200 Myr at the same level of SFR(20Myr). The dashed lines in $z = 5$ and $z = 3$ panels indicate the relation $\text{SFR}(200\text{Myr}) = 0.1 \times \text{SFR}(20\text{Myr})$. At $z = 5$ and 3, the

lower envelope of the distribution follows the dashed line, indicating that in some galaxies star formation is episodic; i.e. the level of $\text{SFR}(20\text{Myr})$ is not maintained over the period of 200 Myr. Therefore, in our simulation, star formation is episodic in some bright LBGs, while in others it is continuous. There is no clear-cut distinction between the two: both episodic and continuous star formation take place. The galaxies that are brighter than $M_V = -21.0$ at $z = 3$ occupy the upper end of the distribution.

8. Metallicity of LBGs

In Figure 11, we show the mean stellar metallicity of galaxies in the simulation vs. intrinsic rest-frame B band absolute magnitude at redshifts $z = 0, 1, 3$, and 5. The result at $z = 0$ was presented in Figure 6 of Paper I with galaxy stellar mass as the x-axis. The solid square points are the median in each magnitude bin, and the error bars are the quartiles. The slanted solid line is the best-fit to observational data compiled by Kobulnicky & Zaritsky (1999) for galaxies at $z = 0 - 0.5$, which shows good agreement with our result at $z = 0$ in the range $-17 \lesssim M_B \lesssim -10$. The distribution at $z = 0$ deviates from the best-fit line at $M_B \lesssim -17$, where we do not have enough statistics in the simulation due to limited box size. However, the flattening of the distribution at bright magnitudes at $z = 3$ is likely to be real. The entire distribution shifts to lower metallicity at higher redshifts. This can be understood from Figure 5 of Paper I, where we showed that the stellar metallicity distribution widens significantly at $z \gtrsim 3$, taking the values ranging from $10^{-4}Z_\odot$ to $3.0Z_\odot$. The physical reason for this effect is that the metallicity is a strong function of local overdensity (Gnedin 1998; Cen & Ostriker 1999). As time progresses, the universe becomes more clumpy, and star formation takes place only in moderate to high overdensity regions where gas is already polluted by metals, resulting in a narrower scatter of metallicity at late times.

The solid box at $z = 3$ indicates the range of metallicity inferred from the oxygen abundance of LBGs (Pettini et al. 2000). The same box is indicated by the dashed line at other redshifts. Our model naturally explains the sub-solar metallicity of LBGs; they take metallicities of $0.1 - 1.0Z_\odot$ because they are the most luminous galaxies at $z = 3$.

The long-dashed horizontal lines at $z = 3$ indicate the typical values of metallicity taken by damped Lyman α systems (DLAs; $Z \approx (1/30)Z_\odot$, Pettini et al. (2001)). LBGs typically have higher metallicity than DLAs. A semianalytic study by Mo et al. (1999) suggests that DLAs are extended, high angular momentum, low surface brightness, rotationally supported disks, while LBGs are low angular momentum, compact, high surface brightness, possibly spheroid systems with high star formation rate. High star formation rate in compact LBGs results in a radial metallicity gradient in a galaxy, with the gas in the outer region hav-

ing much lower metallicity (Shu 2000). The connection between LBGs and DLAs in our simulation will be discussed in detail in a separate paper (Cen et al. 2001).

9. Conclusions

Using a large-scale hydrodynamic simulation, we study the merger tree, the star formation history, the stellar content, and the metallicity of LBGs. We focus our attention on galaxies that are intrinsically brighter than $M_V = -21.0$ at $z = 3$, and investigate the broad range of properties of such galaxies in accordance with recent near-IR observations (Papovich et al. 2001; Pettini et al. 2001; Shapley et al. 2001; Rudnick et al. 2001).

The computed rest-frame V band luminosity function of galaxies at $z = 3$ is presented, and a fair agreement with the observed one is found, given the uncertainties in the simulation, the observations, and the theoretical modeling including the initial mass function and the population synthesis model. We find that the observed luminosity function by Shapley et al. (2001) agrees well with the dust extinguished simulated luminosity function, and that the intrinsic Φ^* could be much larger than the value given by Shapley et al. (2001).

The predicted comoving luminosity density in the rest-frame V band at $z = 3$ is larger than the observed value of Shapley et al. (2001) when integrated down to the current detection limit, but is consistent within the uncertainties when dust extinction is taken into account. A detailed comparison of the total luminosity density at $z = 3$ is hindered by the current detection limit, as the Schechter parameters cannot be determined reliably.

The stellar mass of LBGs that have $M_V \simeq -21.0$ at $z = 3$ lie between $10^{9.5}h^{-1}M_\odot$ and $10^{10.5}h^{-1}M_\odot$, when dust extinction is taken into account. The median stellar mass of all LBGs that are intrinsically brighter than $M_V = -21.0$ at $z = 3$ is $10^{10}h^{-1}M_\odot$, in good agreement with the value inferred from a near-IR observation (Shapley et al. 2001). At $z = 5$, the stellar mass of the progenitors of LBGs ($M_V < -21.0$ at $z = 3$) ranges from $10^{6.9}h^{-1}M_\odot$ to $10^{10.8}h^{-1}M_\odot$, with a median of $10^{8.6}h^{-1}M_\odot$.

We find that the majority of LBGs brighter than $M_V = -23$ at $z = 3$ fall into groups and clusters of galaxies by $z = 0$. Roughly one half of LBGs with $-23 \lesssim M_V \lesssim -22$ merge into groups/clusters of galaxies, while the other half evolve into typical L^* galaxies with $M_{\text{stellar}} \approx 10^{11}M_\odot$. Present day galaxies with $M_{\text{stellar}} \gtrsim 10^{11}M_\odot$ typically have a few LBGs as their progenitors brighter than $M_V = -21.0$, with $M_{\text{stellar}} \gtrsim 10^{10}M_\odot$. Descendants of LBGs at the present epoch formed $\approx 30\%$ of their stellar mass by $z = 3$, and $\approx 50\%$ of their present stellar population is 10 Gyr old. The existence of a significant old stellar population suggests that LBGs may be the precursors of the present day spheroids.

Our simulation suggests that LBGs that are brighter than $M_V = -23$ at $z = 3$ have experienced a burst of star formation ($\geq 100M_\odot/\text{yr}$) within 500 Myr prior to $z = 3$, often lasting for a period of ≈ 100 Myr. We also find that the majority of LBGs brighter than $M_V = -21.0$ have extended star formation activity at higher redshifts ($z = 3 - 10$) over a period of 1 Gyr, resulting in a median stellar mass of $10^{10}h^{-1}M_\odot$ at $z = 3$, in accordance with the picture proposed by Steidel et al. (1996). There seems to be no clear-cut choice between the two star formation scenarios: the bright LBGs in our simulation exhibit both instantaneous and continuous star formation activity. Our result seems to be in qualitative agreement with the star formation histories inferred from recent near-IR observations of LBGs (Papovich et al. 2001; Shapley et al. 2001). The stellar content and the merger history we observe in the simulation is not consistent with the picture that LBGs are low-mass starbursting objects which later evolve into low-mass spheroids at $z = 0$ (Lowenthal et al. 1997; Sawicki & Yee 1998; Somerville et al. 2001).

We argued in Paper I that the global star formation rate in the simulation increases toward higher redshifts up to $z \sim 8$. Together with the results presented in this paper, the existence of high star formation rate galaxies at high-redshift seems to be a generic prediction of the CDM model. It is an important future task to investigate the link between these galaxies in the simulation and the observation of high-redshift galaxies such as the Hubble Deep Field (Williams et al. 1996) and the future Next Generation Space Telescope (Stockman et al. 1996).

Our results on the star formation rates of high-redshift galaxies are in good agreement with the previous studies by Davé et al. (1999) and Weinberg et al. (2000). This is not surprising given that the simulations used in both studies adopt a similar star formation recipe, although the spatial and the mass resolutions are very different.

The sub-solar metallicity of LBGs at $z = 3$ is naturally predicted by our simulation. The entire luminosity-metallicity distribution shifts to lower metallicity at higher redshifts. If indeed DLAs have metallicity of $\sim (1/30)Z_\odot$ (Pettini et al. 2000), then LBGs typically have higher metallicity than DLAs at $z = 3$. The connection between LBGs and DLAs in our simulation will be studied in a separate paper (Cen et al. 2001).

This paper is based on the thesis work of K.N. at Princeton University. The author is grateful to Drs. Jeremiah P. Ostriker, Renyue Cen, and Masataka Fukugita for the collaboration on the two previous papers (Paper I & II), and for advice, support and important scientific input to the present work. Drs. Renyue Cen and Jeremiah P. Ostriker are thanked for providing the simulation for the present work. We thank Dr. Chuck Steidel for useful discussions and wonderful Spitzer Lecture Series given at the Peyton Hall of Princeton Uni-

versity in May 2001, which largely inspired this work. K.N. is grateful to Alice Shapley for making the draft of an unpublished paper available, and to Kurt Adelberger for the U_n , G , \mathcal{R} filter functions. We thank Michael Strauss for useful comments on the draft. This work was supported in part by grants AST 98-03137 and ASC 97-40300. K.N. is supported in part by the Physics Department of Princeton University.

REFERENCES

- Adelberger, K. L., Steidel, C. C., Giavalisco, M., Dickinson, M. E., Pettini, M., & Kellogg, M. 1998, *ApJ*, 505, 18
- Aguirre, A., Hernquist, L., Schaye, J., Weinberg D. H., Katz, N., & Gardner, J. 2001, *ApJ*, in press (astro-ph/0006345)
- Baugh, C. M., Cole, S., Frenk. C. S., & Lacey, C. G., 1998, *ApJ*, 498, 504
- Blanton, M. R., et al. 2000, *AJ*, 121, 2358
- Blanton, M., Cen, R., Ostriker, J. P., & Strauss, M. A. 1999, *ApJ*, 522, 590
- Bruzual, A. G. & Charlot, S., 1993, *ApJ*, 405, 538
- Calzetti, D., Armus, L., Bohlin, R. C., Kinney, A. L., Koornneef, J., & Storchi-Bergmann, R. 2000, *ApJ*, 533, 682
- Calzetti, D. 1997, *AJ*, 113, 162
- Cen, R., et al. 2001, in preparation
- Cen, R. and Ostriker, J. P. 1999, *ApJ*, 519, L109
- Cross, N., et al., 2001, *MNRAS*, 324, 825
- Davé, R., Hernquist, L., Katz, N., & Weinberg, D. H. 1999, the Proceedings of Rencontres Internationales de l'IGRAP, Clustering at High Redshift, Marseille (astro-ph/9910220)
- Eisenstein, D. J. & Hut, P. 1998, *ApJ*, 498, 137
- Friaca, A. C. S. and Terlevich, R. J. 1999, *MNRAS*, 305, 90
- Fukugita, M., Hogan, C. J., Peebles, P. J. E., 1999, *ApJ*, 503, 518

- Giavalisco, M., Steidel, C. C., Adelberger, K. L., Dickinson, M. E., Pettini, M., & Kellogg, M. 1998, *ApJ*, 503, 543
- Giavalisco, M., Steidel, C. C., Macchetto, F. D. 1996, 470, 189
- Gnedin, N. Y. 1998, *ApJ*, 294, 407
- Gould, A., Bahcall, J. N., & Flynn, C. 1996, *ApJ*, 465, 759
- Governato, F., Ghigna, S., Moore, B., Quinn, T., Stadel, J., & Lake, G. 2001, *ApJ*, 547, 555
- Kobulnicky, H. A. & Zaritzky, D. 1999, *ApJ*, 1999, 511, 118
- Lowenthal, J. D., et al. 1997, *ApJ*, 481, 673
- Mo, H. J., Mao, S., & White, S. D. M. 1999, *MNRAS*, 304, 175
- Mo, H. J. & Fukugita, M. 1996, *ApJ*, 467, L9
- Nagamine, K., Fukugita, M., Cen, R., & Ostriker, J. P. 2001b, *MNRAS*, in press (astro-ph/0102180; Paper II)
- Nagamine, K., Fukugita, M., Cen, R., & Ostriker, J. P. 2001a, *ApJ*, in press (astro-ph/0011472; Paper I)
- Papovich, C., Dickinson, M., & Ferguson, H. C., 2001, *ApJ*, in press (astro-ph/0105087)
- Pettini, M., et al. 2001, *ApJ*, 554, 981
- Pettini, M., Steidel, C. C., Adelberger, K. L., Dickinson, M., & Giavalisco, M. 2000, *ApJ*, 528, 96
- Rees, M. J. & Ostriker, J. P. 1977, *MNRAS*, 179, 541
- Roberts, M. S. & Haynes, M. P. 1994, *ARA&A*, 32, 115
- Rudnick, G., et al. 2001, *AJ*, submitted (astro-ph/0106074)
- Salpeter, E. E., 1955, *ApJ*, 121, 161
- Sawicki, M. & Yee, H. K. C., 1998, *AJ*, 115, 1329
- Shapley, A. E., Steidel, C. C., Adelberger, K. L., Dickinson, M., Giavalisco, M., & Pettini, M., 2001, *ApJ*, in press (astro-ph/0107324)
- Shu, C. 2000, *A&A*, 354, 815

- Silk, J. 1977, ApJ, 211, 638
- Somerville, R. S., Primack, J. R., & Faber, S. M., 2001, MNRAS, 320, 504
- Steidel, C. C., Adelberger, K. L., Giavalisco, M., Dickinson, M. & Pettini, M. 1999, ApJ, 519, 1
- Steidel, C. C., Adelberger, K. L., Dickinson, M., Giavalisco, M., Pettini, M., Kellogg, M. 1998, ApJ, 492, 428
- Steidel, C. C., Giavalisco, M., Pettini, M., Dickinson, M. E., & Adelberger, K. L., 1996, ApJ, 462, L17
- Steidel, C. C., Pettini, M., & Hamilton, D., 1995, AJ, 110, 2519
- Steidel, C. C. & Hamilton, D., 1992, AJ, 104, 941
- Stockman, H. S., Mather, J. C., Smith, E., Thronson, H., Margulis, M., Lillie, C. 1996, AAS, 189.6001
- Weinberg, D. W., Hernquist, L., & Katz, N. 2000, preprint (astro-ph/0005340)
- Williams R. E., et al., 1996, AJ, 112, 1335

Table 1. Schechter Parameters in Rest-frame V Band

Quantities	$z=0$	$z=0.3$	$z=0.5$	$z=1$	$z=2$	$z=3$	$z=5$
M_V^*	-22.15	-22.59	-22.68	-22.64	-22.50	-22.05	-21.17
ϕ^*	0.83	0.90	0.97	1.17	1.70	2.70	5.50
\mathcal{L}_V	1.73	2.82	3.29	3.82	4.89	5.10	4.66

Note. — Parameters of the Schechter functions in rest-frame V band before taking dust extinction into account. The faint-end slope α is fixed to -1.15 in all cases. See text for the method of fitting M_V^* [mag] and $\phi^*[10^{-2}h^3 \text{Mpc}^{-3}]$. \mathcal{L}_V is in units of $[10^8 L_{\odot,V} \text{Mpc}^{-3}]$ with $h = 0.67$. Similar table for B band was presented in Paper II.

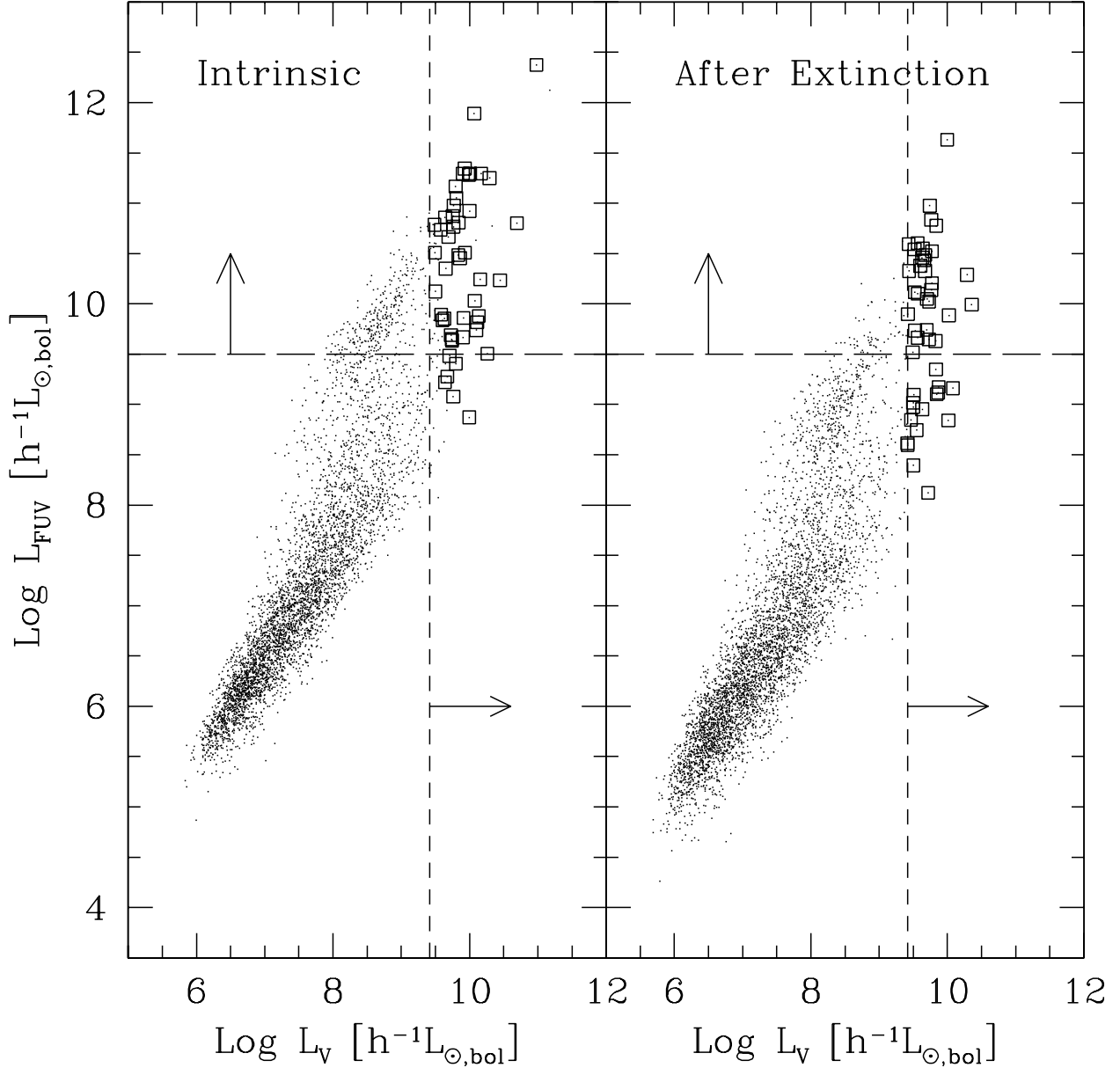


Fig. 1.— Rest-frame V band luminosity vs. rest-frame far-UV luminosity (summing all luminosity below 1700 \AA) of galaxies at $z = 3$ in the simulation. The left panel shows the intrinsic luminosity (before dust extinction), and the right panel is after a dust extinction model is applied. The magnitude limit ($K_s = 22.5$) of a near-IR observation (Shapley et al. 2001) is indicated by the vertical short-dashed line and the arrow toward right. Open squares indicate galaxies that are brighter than this magnitude limit after dust extinction. The horizontal long-dashed line and the upward arrow roughly indicate the far-UV selection criteria of $\mathcal{R} < 25.5$ (Shapley et al. 2001). Note that the rest-frame V band selected sample takes a wider range of values in far-UV luminosity.

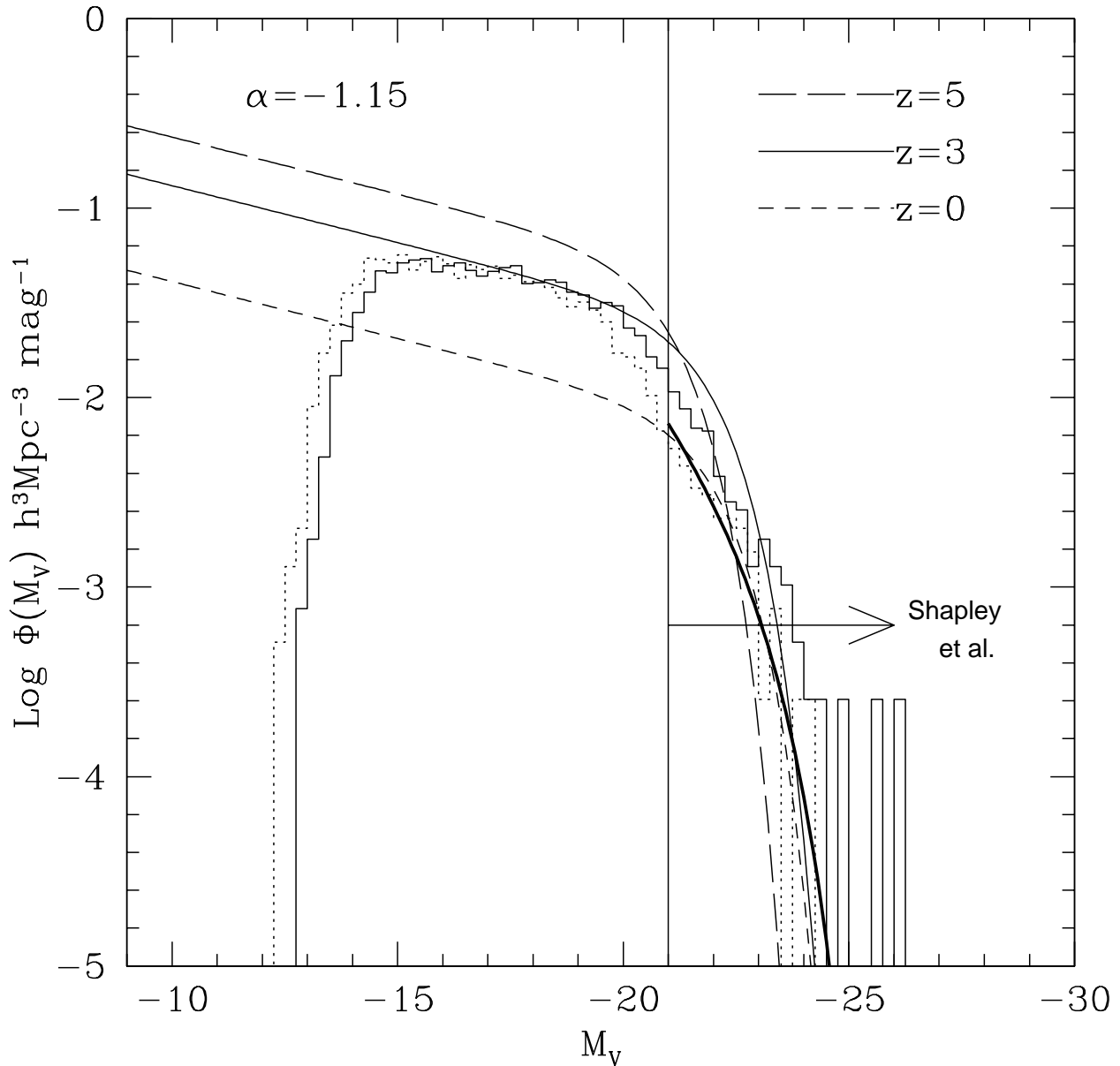


Fig. 2.— Solid histogram shows the rest-frame V band luminosity function derived from the simulation at $z = 3$ (before dust extinction). Short-dashed, solid, and long-dashed curves show the Schechter function fit at $z = 0, 3$, and 5 , respectively. See text for the fitting method. The Schechter parameters are summarized in Table 1. The heavy solid line is the observed luminosity function by Shapley et al. (2001), and their detection limit ($M_V = -21.0$) in near-IR is shown by the vertical solid line and the arrow. The dotted histogram is the dust extinguished luminosity function in the simulation. Current surveys sample only the bright-end of the luminosity function at $z = 3$, and are in good agreement with the simulated one with dust extinction.

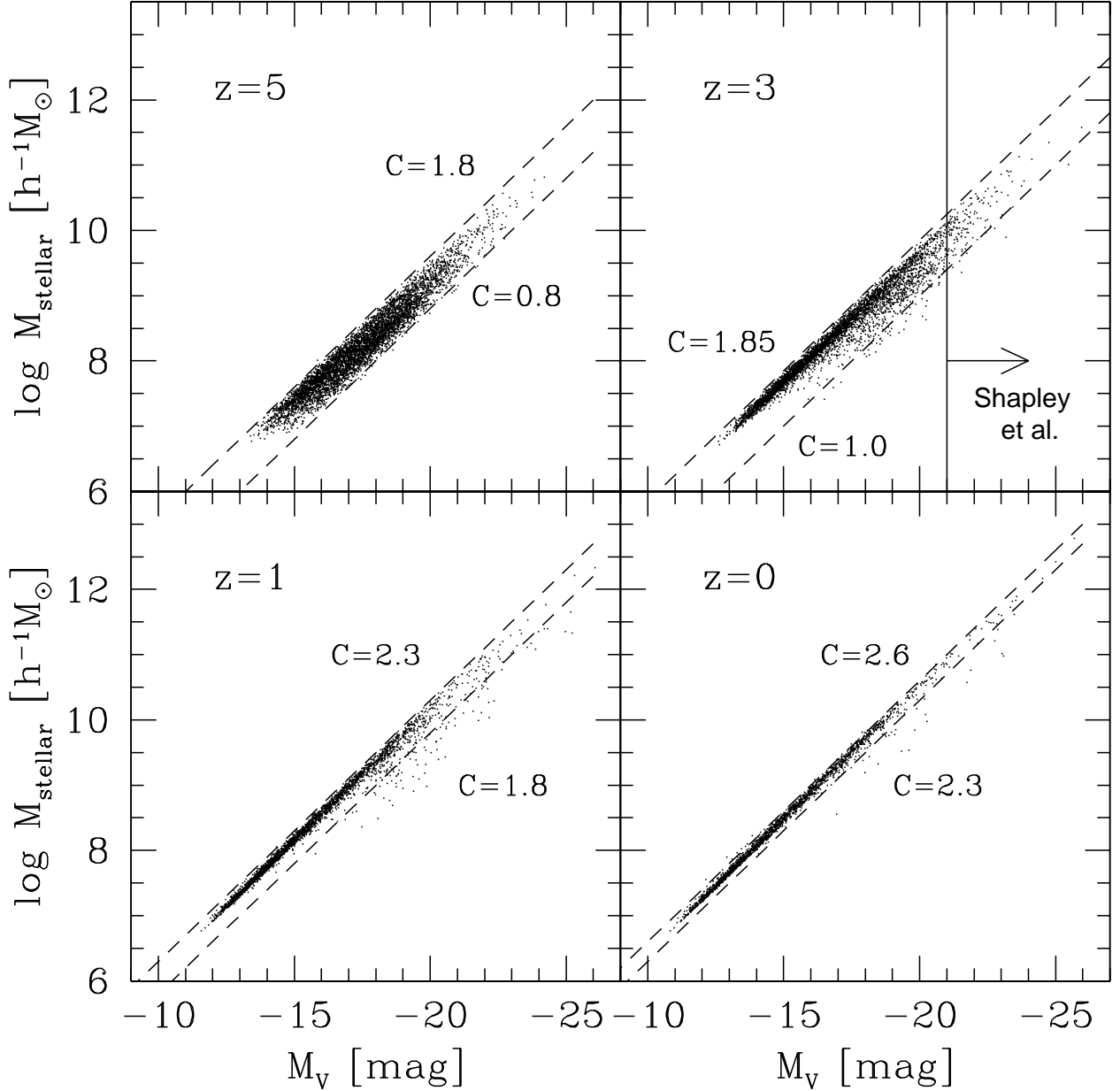


Fig. 3.— Stellar mass of galaxies vs. rest-frame V band absolute magnitude (before dust extinction) at $z = 5, 3, 1$, and 0 . Each point in the figure represents one galaxy in the simulation. The dashed lines are drawn by hand to roughly indicate the locus of the distribution, together with the values of the constant C , where $\log M_{\text{stellar}} = -0.4M_V + C$ and M_{stellar} is in units of $[h^{-1}M_{\odot}]$. The entire distribution shifts to the upper left direction from high to low-redshift, as galaxies become more massive and less luminous. The wider distribution at high-redshift indicates more active star formation activity and its variety. The detection limit of $M_V = -21.0$ (Shapley et al. 2001) is indicated by the vertical solid line and the arrow in $z = 3$ panel. The median stellar mass of all galaxies above this detection limit is $10^{10}h^{-1}M_{\odot}$.

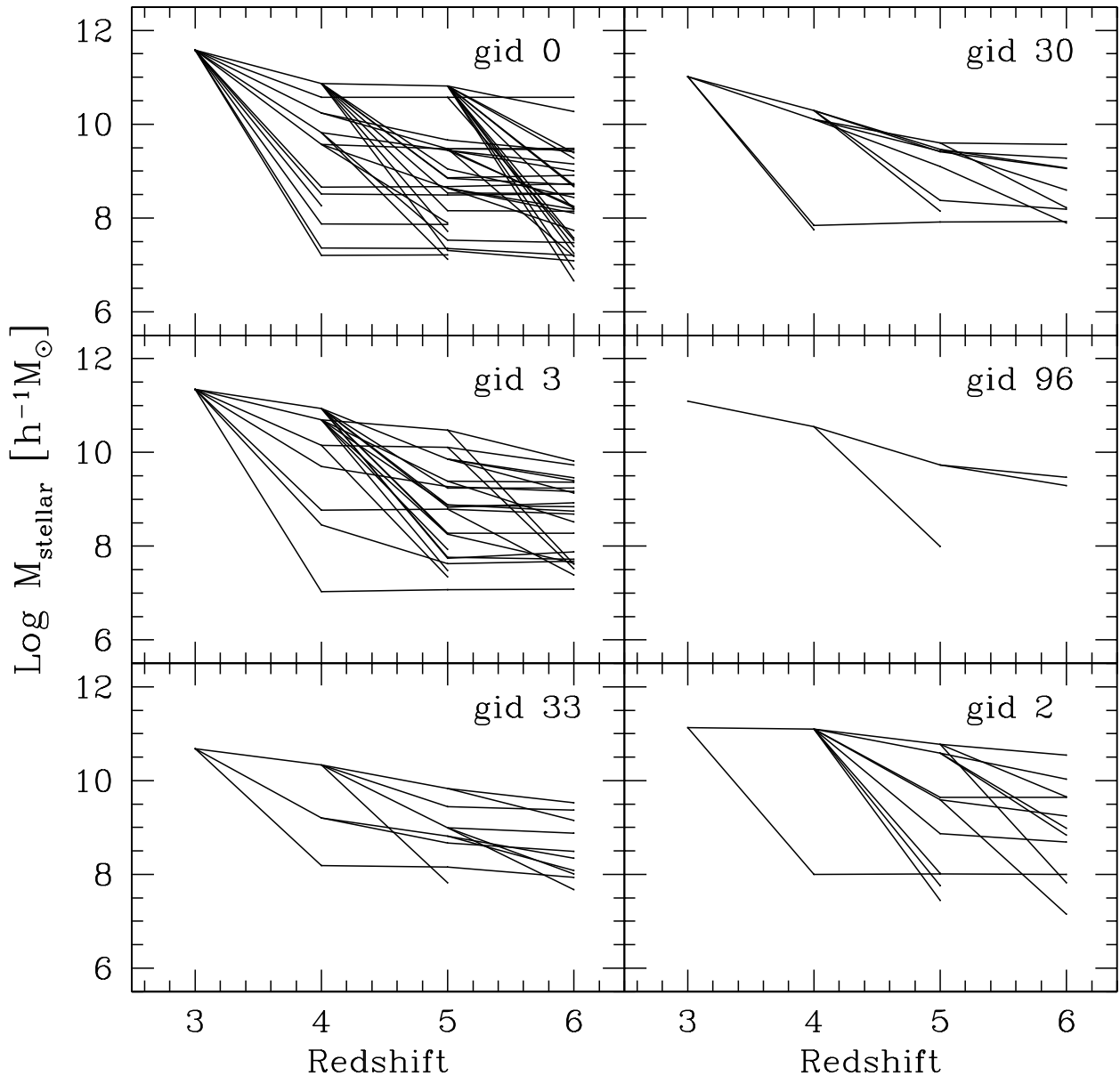


Fig. 4.— Merger trees of the brightest LBGs (intrinsic luminosity $M_V < -23.5$ at $z = 3$) are shown in the order of their rest-frame V band luminosity at $z = 3$ from top left to bottom right. The ordinate is the stellar mass of galaxies. Each leg in the figure connects two objects before and after a merger event that took place in between the two redshifts. The corresponding composite star formation histories are shown in Figure 5. See text for the discussion on each galaxy.

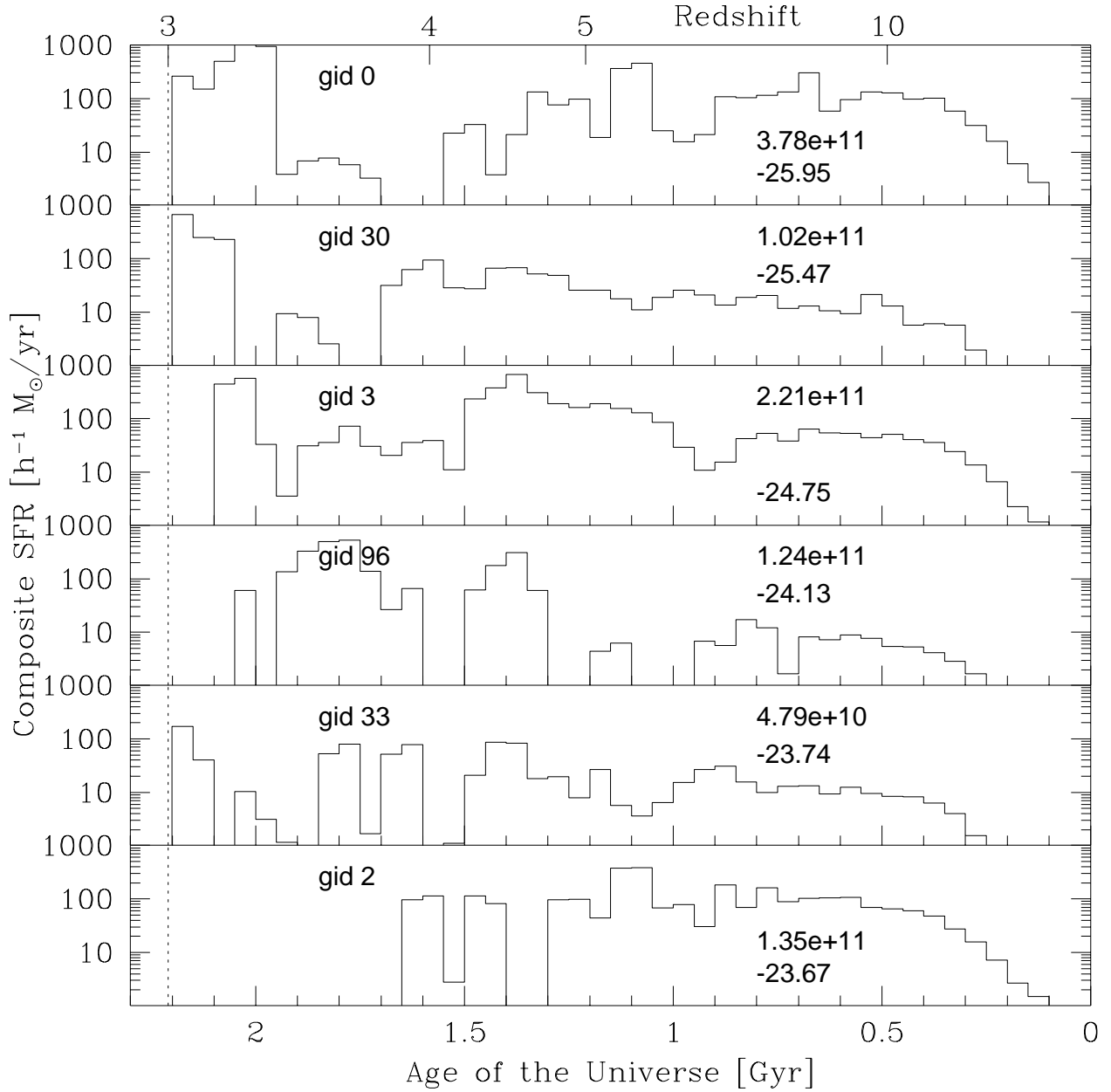


Fig. 5.— Composite star formation histories of LBGs in Figure 4 in the order of the rest-frame V band luminosity at $z = 3$ from top to bottom. The bin size of the histogram is 50 Myr. Note that this is the composite star formation rate of all progenitors which fall into a given LBG at $z = 3$. The values of the stellar mass (in units of M_{\odot}) and the rest-frame V band absolute magnitude of the object at $z = 3$ are given in each panel. The vertical dotted line on the left indicates $z = 3$. See text for the discussion for each galaxy.

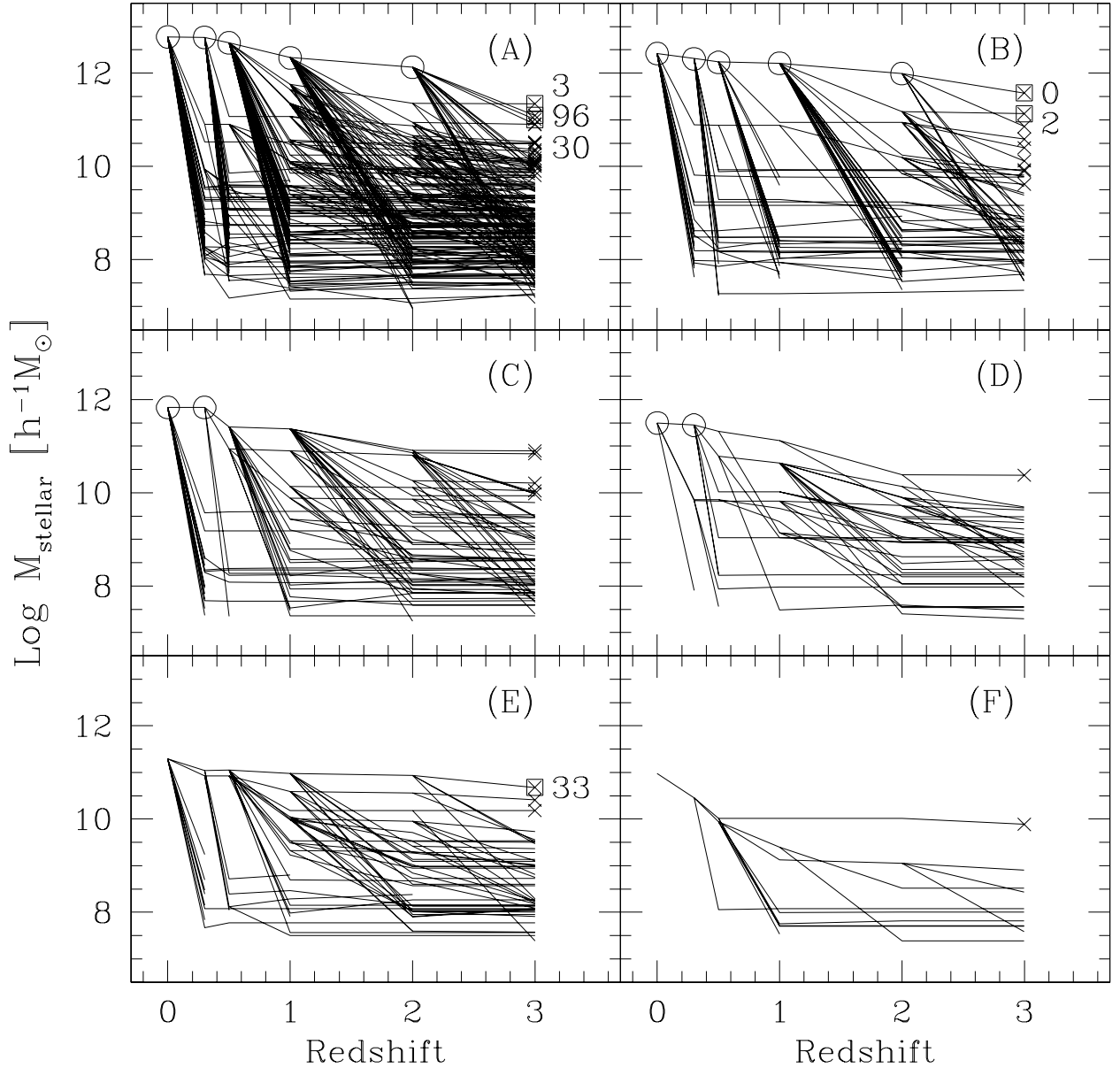


Fig. 6.— Merger trees of the present day cluster, groups, and L^* galaxies are shown in the order of their stellar mass at $z = 0$ from top to bottom. The ordinate is the stellar mass of galaxies. The LBGs that are brighter than $M_V = -21.0$ are indicated by the crosses at $z = 3$. The open circles in panels (A)–(D) indicate that the objects are suffering from the overmerging problem in the simulation, and represent clusters/groups of galaxies as a whole. The corresponding star formation histories are shown in Figure 7. See text for the discussion on each galaxy.

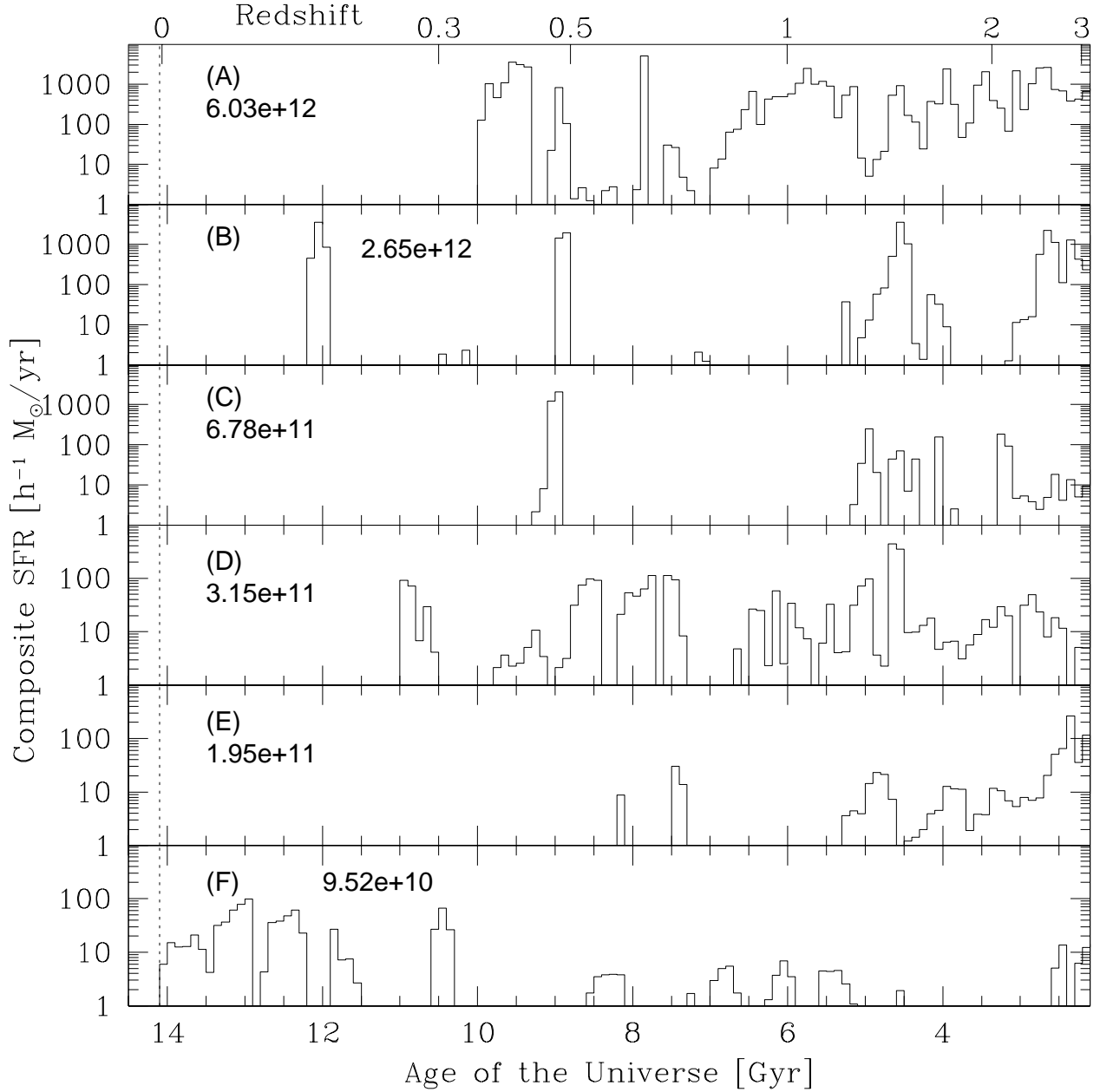


Fig. 7.— Composite star formation histories of objects shown in Figure 6 as a function of the age of the universe. The bin size of the histogram is 100 Myr. Note that the histograms are the composite star formation rate of all progenitors that fall into the same object at $z = 0$. The value of the stellar mass of each object at $z = 0$ is shown in each panel in units of $h^{-1}M_{\odot}$. The vertical dotted line indicates the present epoch in the simulation. See text for the discussion on each galaxy.

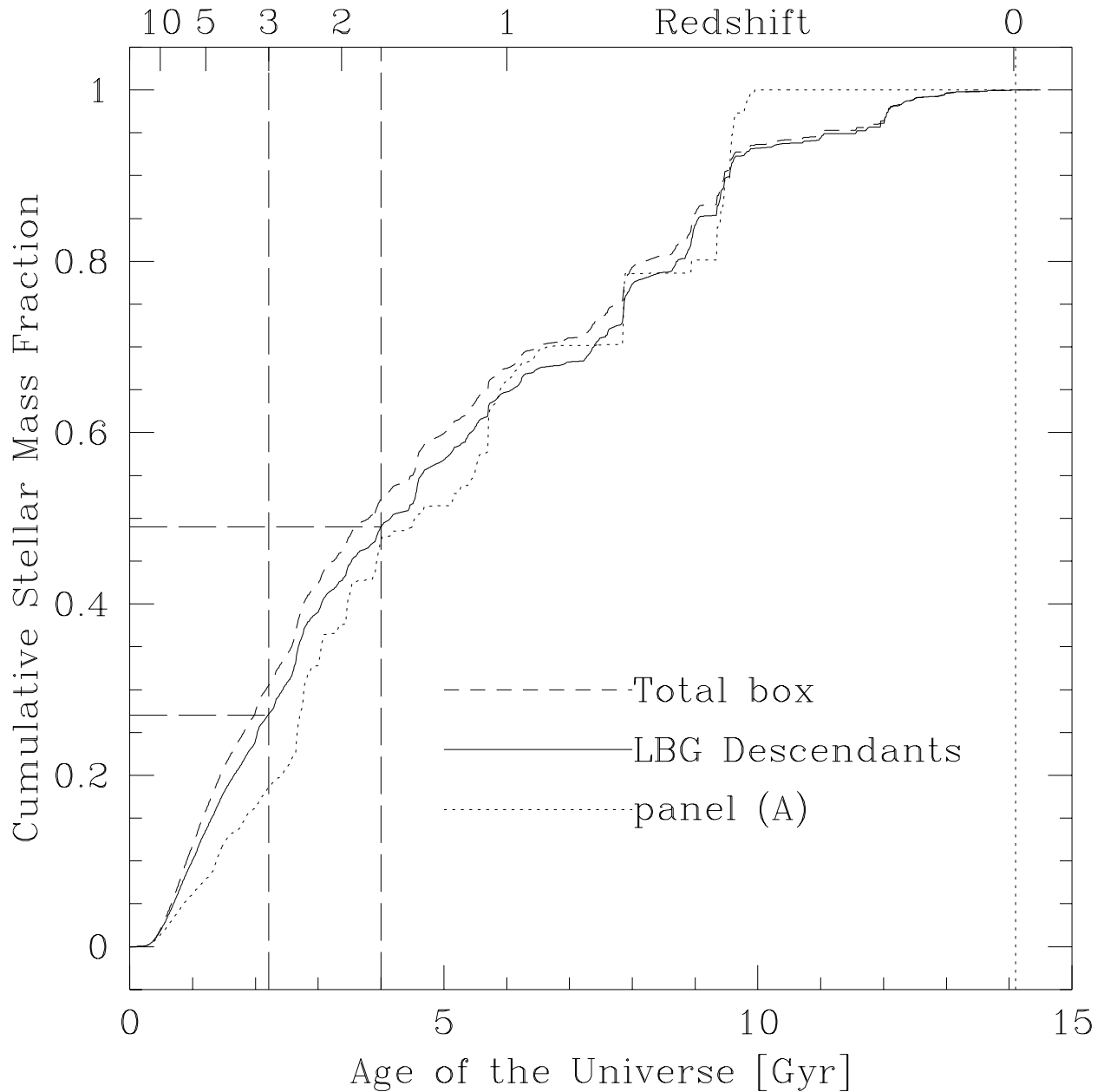


Fig. 8.— Cumulative stellar mass fraction as a function of the age of the universe and redshift for the total box (short dashed), descendants of the LBGs which are brighter than $M_V = -21.0$ at $z = 3$ (solid), and the cluster shown in panel (A) of Figure 6. The long dashed lines indicate that the present day descendants of LBGs have formed $\sim 30\%$ of their stellar mass by $z = 3$, and $\sim 50\%$ of their present day stellar population is 10 Gyr old, in favor of the scenario that LBGs are the precursors of the present day spheroids.

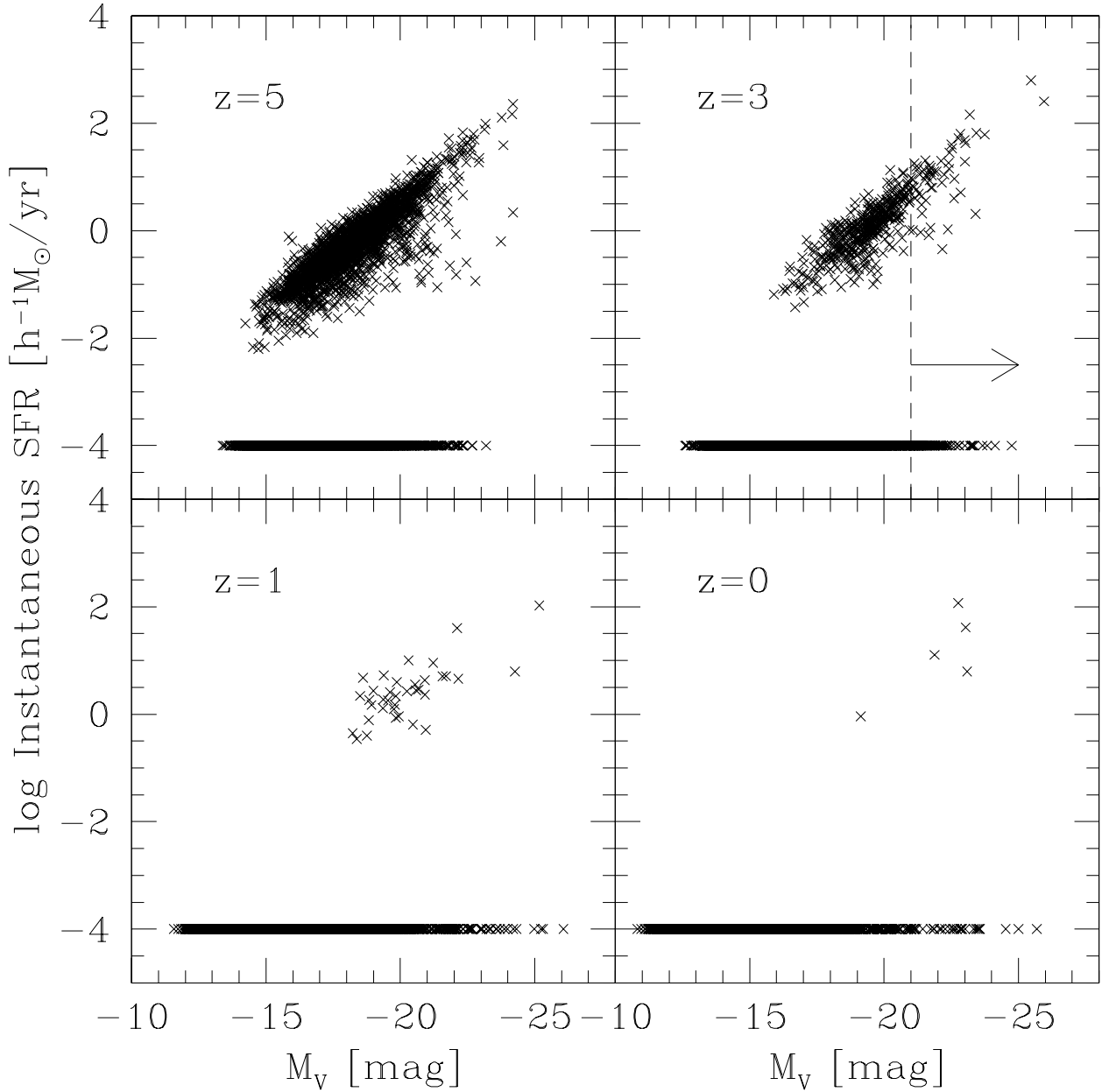


Fig. 9.— Instantaneous star formation rate of galaxies at $z = 0, 1, 3,$ and 5 as a function of rest-frame V band absolute magnitude (before dust extinction), calculated by averaging over 20 Myr at each epoch. Those which are assigned $10^{-4}[h^{-1}M_{\odot}/\text{yr}]$ happen to have no star formation at that epoch, due to the intermittent nature of the star formation in the simulation. The vertical dashed line and the arrow at $z = 3$ indicates the detection limit of $M_V = -21.0$ (Shapley et al. 2001).

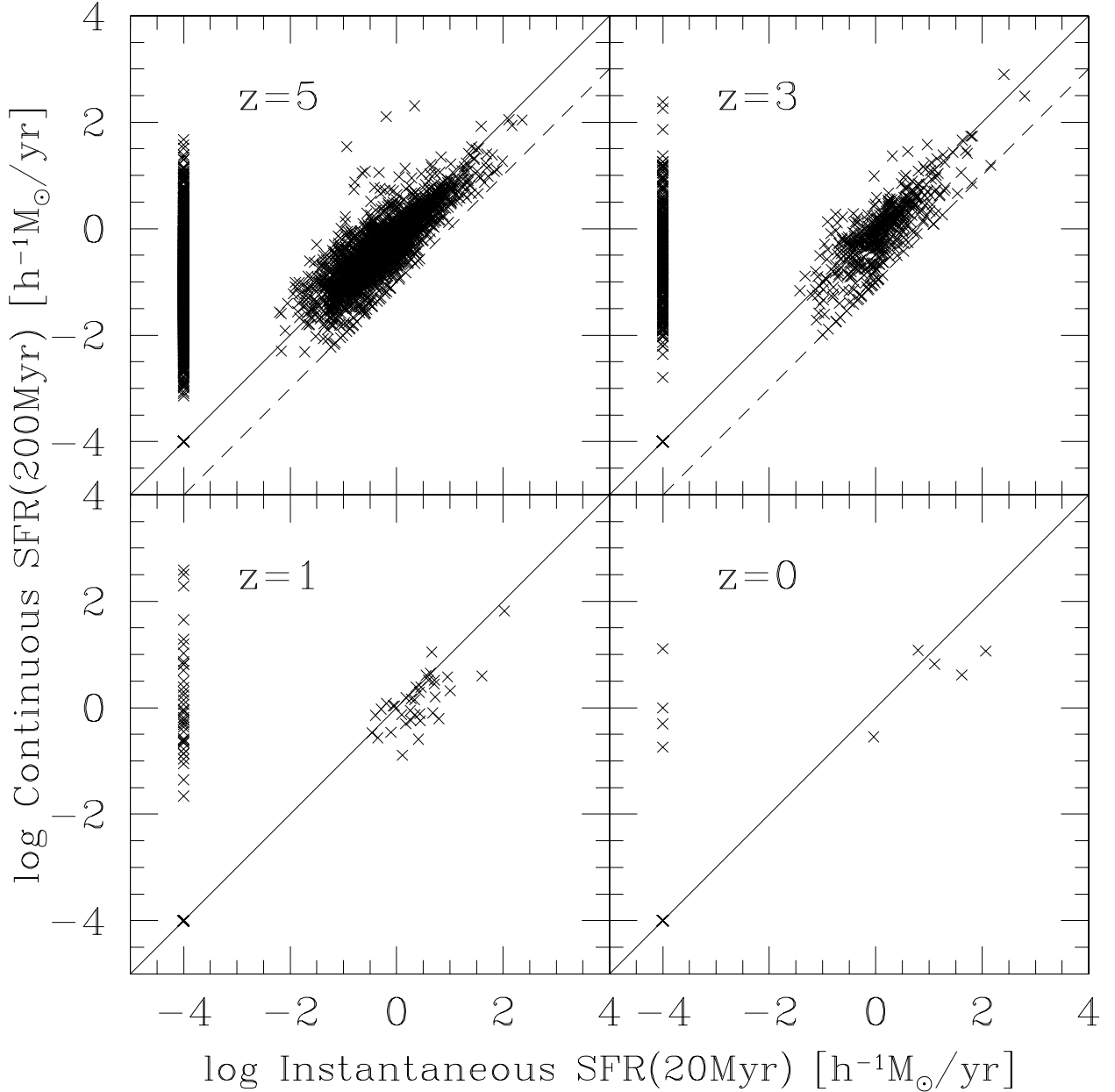


Fig. 10.— ‘Instantaneous SFR’ (averaged over 20 Myr) vs. ‘Continuous SFR’ (averaged over 200 Myr) of galaxies in the simulation. The diagonal solid line indicates where the two SFRs take the same value; i.e. the star formation is continuous over at least 200 Myr at the same level of SFR(20Myr). The dashed lines in $z = 5$ and $z = 3$ panels indicate the relation $\text{SFR}(200\text{Myr}) = 0.1 \times \text{SFR}(20\text{Myr})$. Bright LBGs occupy the upper region of the distribution. Some LBGs have episodic star formation, while others form stars continuously. The galaxies which are assigned $10^{-4} [h^{-1} M_{\odot}/\text{yr}]$ happen to have no star formation at that epoch, due to the intermittent nature of the star formation in the simulation.

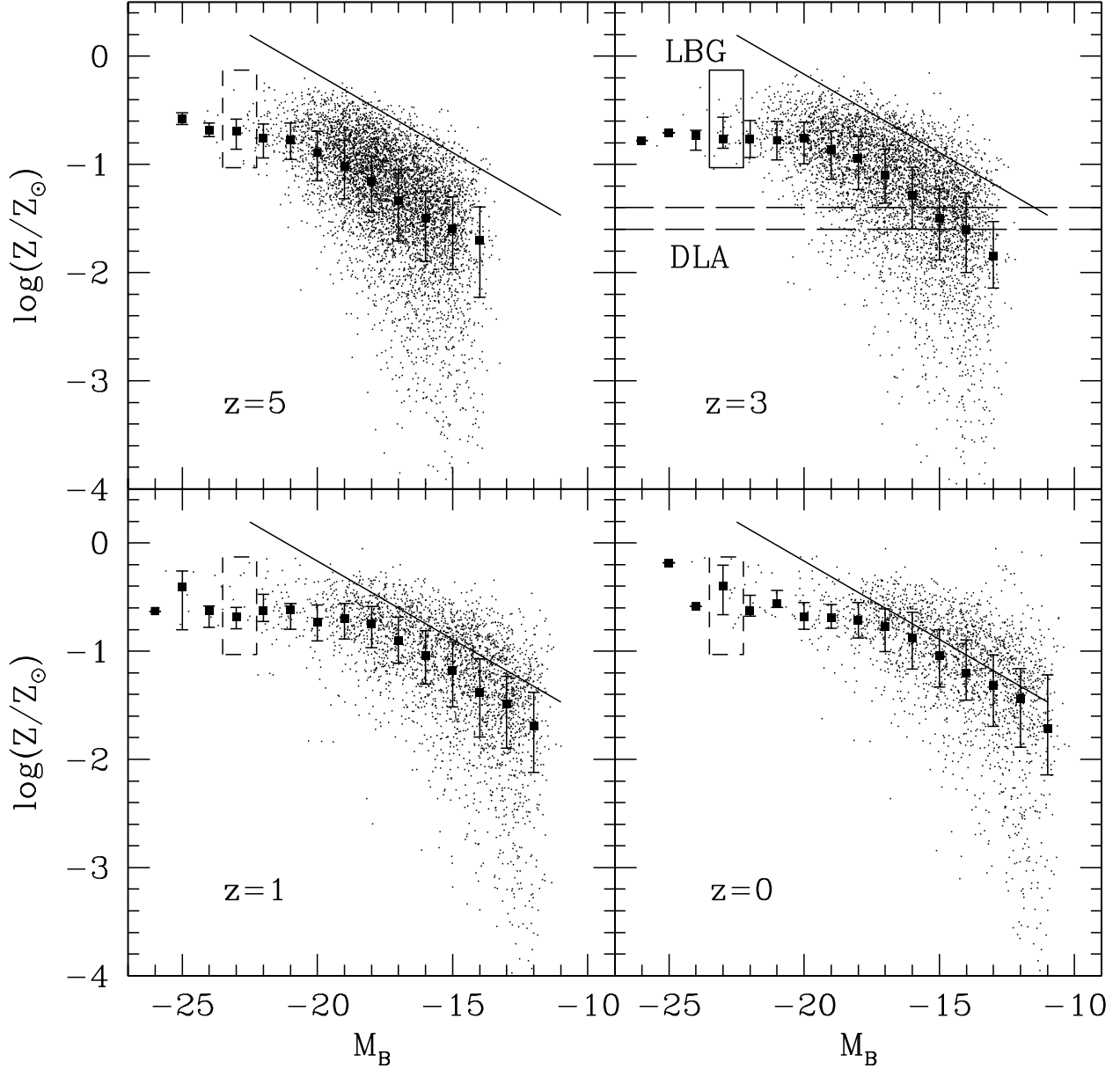


Fig. 11.— Mean stellar metallicity of galaxies vs. rest-frame B band absolute magnitude (intrinsic) at redshifts $z = 5, 3, 1,$ and 0 . The solid square points are the median in each magnitude bin, and the error bars are the quartiles. The solid box at $z = 3$ indicates the range of metallicity of the LBGs given by Pettini et al. (2001). The same box is indicated by the dashed line at other epochs. The long-dashed horizontal lines at $z = 3$ indicate the typical values of metallicity taken by the damped Lyman α systems ($\sim 1/30Z_\odot$; Pettini et al. 2001). The slanted solid line is the best-fit to the observational data compiled by Kobulnicky & Zaritsky (1999) for galaxies at $z = 0 - 0.5$. The entire distribution shifts to lower metallicity at higher redshifts.